Available online at www.sciencedirect.com
SCIENCE DIRECT®
Journal of Sound and Vibration 289 (2006) 1019–1044
JOURNAL OF SOUND AND VIBRATION
www.elsevier.com/locate/jsvi

Dynamic modeling and identification of a slider-crank mechanism

Jih-Lian Ha[a], Rong-Fong Fung[b,*], Kun-Yung Chen[b], Shao-Chien Hsien[b]

[a]*Department of Mechanical Engineering, Far East College, 49 Chung-Hua Road, Shin-Shi, Tainan, Taiwan 744, ROC*
[b]*Department of Mechanical and Automation Engineering, National Kaohsiung First University of Science and Technology, 1 University Road, Yenchau, Kaohsiung, Taiwan 824, ROC*

Received 4 May 2004; received in revised form 21 January 2005; accepted 7 March 2005
Available online 3 June 2005

Abstract

In this paper, Hamilton's principle, Lagrange multiplier, geometric constraints and partitioning method are employed to derive the dynamic equations of a slider-crank mechanism driven by a servomotor. The formulation is expressed by only one independent variable and considers the effects of mass, external force and motor electric inputs. Comparing the dynamic responses between the experimental results and numerical simulations, the dynamic modeling gives a wonderful interpretation of a slider-crank mechanism. The parameters of many industrial machines are difficult to obtain if these machines cannot be taken apart. In this paper, a new identification method based on the real-coded genetic algorithm (RGA) is presented to identify the parameters of a slider-crank mechanism. The method promotes the calculation efficiency very much, and is calculated by the real-code without the operations of encoding and decoding. The results of numerical simulations and the experiments prove that the identification method is feasible. Finally, the experimental results by the RGA and the recursive least squares (RLS) are also compared.

1. Introduction

A slider-crank mechanism is widely used in gasoline and diesel engines, and has been studied extensively in the past three decades. The responses of the system found by Viscomi and Ayre [1]

*Corresponding author. Tel.: +886 7 601 1000x2221; fax: +886 7 601 1013.
E-mail address: rffung@ccms.nkfust.edu.tw (R.-F. Fung).

0022-460X/$ - see front matter © 2005 Elsevier Ltd. All rights reserved.
doi:10.1016/j.jsv.2005.03.011

Nomenclature

B_m	motor damping coefficient
F_E	external disturbance force acting on the slider
F_B	friction force
F_f	fitness function
g	gravity acceleration
i_q	torque current command
J_m	motor moment inertia
K_t	motor torque constant
l	the length of the rod CM
$\mathbf{M}$	the mass matrix
m_1	the mass of the disk
m_2	the mass of the rod CM
m_3	the mass of the slider
$\mathbf{N}$	the nonlinear vector
$\mathbf{Q}$	the vector of generalized coordinates
r	the radius of the disk
T	the kinetic energy of a slider-crank mechanism
t	time
V	the potential energy of a slider-crank mechanism
X_B	the displacement of slider B
ϕ	the angle between rod CD and X-axis
λ	Lagrange multiplier
μ	the coefficient of friction
θ	the angle position of the disk
τ	the load torque

are dependent upon five parameters: the length, mass, damping, external piston force and frequency. The steady-state responses of the flexible connecting rod of a slider-crank mechanism with time-dependent boundary effect were obtained by Fung [2]. A slider-crank mechanism with constantly rotating speed was controlled by Fung et al. [3]. The mathematical model of the coupled mechanism of a slider-crank mechanism was obtained by Lin et al. [4], where the system is actuated by a field-oriented control permanent magnet (PM) synchronous servomotor.

However, the dynamic formulations of a slider-crank mechanism with one degree of freedom have more than one independent variable in the past researches [3,4]. In this study, the dynamic formulation is expressed by only one independent variable of rotation angle. Moreover, its dynamic responses are compared well with the experimental results.

Genetic algorithm was defined by John Holland in 1975 [5]. It is a search process based on natural selection, and is now used as a tool for searching the large, poorly understood spaces that arise in many application areas of science and engineering. Although it has recently found extensive applications, most have low calculation efficiency because the procedure of the GA [6,7] must use the operations of encoding and decoding. In addition, the parameters of many industrial machines are difficult to obtain because these machines cannot be taken apart. It is more natural to represent the genes directly as real numbers. Because the method is calculated by real code, it can shorten the calculating time. Therefore, the RGA promotes the calculation efficiency very much. In order to solve the arduous problem, the real-coded genetic algorithm (RGA) [8–10] is employed to find the optimal identified parameters of a slider-crank mechanism in this study.

This study successfully demonstrates that the dynamic formulation can give a wonderful interpretation of a slider-crank mechanism by comparing it with the dynamic responses of the experimental results. Furthermore, a new identified method using the RGA is proposed, and it is confirmed that the method can perfectly search the parameters of a slider-crank mechanism through the numerical simulations and experiments.

2. Dynamic formulation of a slider-crank mechanism

A slider-crank mechanism is a single-looped mechanism with a very simple construction shown in Fig. 1(a); the experimental equipment of a slider-crank mechanism is shown in Fig. 1(b). It consists of three parts: a rigid disk, which is driven by a servomotor, a connecting rod and a slider.

2.1. Dynamic modeling

2.1.1. Geometric equations

Fig. 1(a) shows the physical model of a slider-crank mechanism, where the mass center and the radius of the rigid disk are denoted as point "O" and length "r", respectively. The length of the connected rod AB is denoted by "l". The angle θ is between OA and the X-axis, while the angle ϕ is between the rod AB and the X-axis. In the OXY plane, the geometric positions of gravity centers of the rigid disk, connected rod and slider, respectively, are as follows:

$$x_{1cg} = 0, \quad y_{1cg} = 0, \tag{1}$$

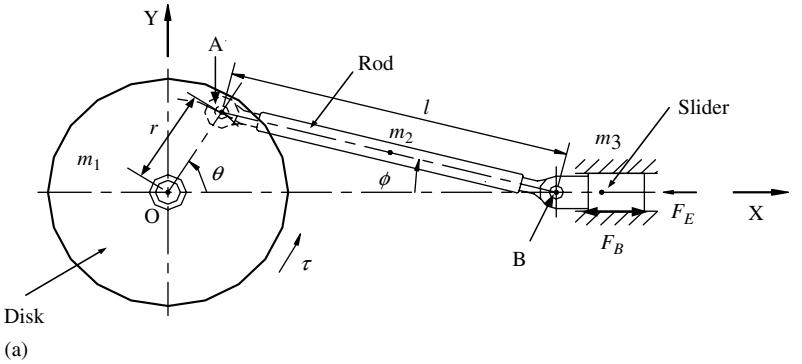

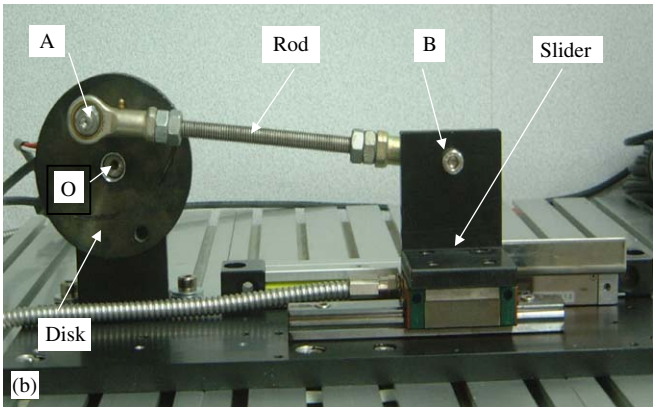

Fig. 1. The slider-crank mechanism. (a) The physical model of a slider-crank mechanism, (b) the experiment equipment of a slider-crank mechanism.

$$x_{2cg} = r\cos\theta + \tfrac{1}{2}l\cos\phi, \quad y_{2cg} = \tfrac{1}{2}l\sin\phi, \tag{2}$$

$$x_{3cg} = r\cos\theta + l\cos\phi, \quad y_{3cg} = 0. \tag{3}$$

The mechanism has a constrained condition as follows:

$$r\sin\theta = l\sin\phi. \tag{4}$$

The angle ϕ can be found from Eq. (4) as

$$\phi = \sin^{-1}\left(\frac{r}{l}\sin\theta\right). \tag{5}$$

2.1.2. Kinematic analysis

In the kinematic analysis, taking the first and second derivates of the displacement of slider B with respect to time, the speed and acceleration of slider B are as follows:

$$\dot{x}_B = -r\dot{\theta}\sin\theta - l\dot{\phi}\sin\phi, \tag{6}$$

$$\ddot{x}_B = -r\ddot{\theta}\sin\theta - r\dot{\theta}^2\cos\theta - l\ddot{\phi}\sin\phi - l\dot{\phi}^2\cos\phi. \tag{7}$$

Similarly, the angular velocity $\dot{\phi}$ and acceleration $\ddot{\phi}$ are obtained as follows:

$$\dot{\phi} = \frac{r\dot{\theta}\cos\theta}{l\cos\phi}, \tag{8}$$

$$\ddot{\phi} = \frac{r\ddot{\theta}\cos\phi\cos\theta + r\dot{\theta}\dot{\phi}\cos\theta\sin\phi - r\dot{\theta}^2\sin\theta\cos\phi}{l\cos^2\phi}. \tag{9}$$

2.1.3. Field-oriented PM synchronous motor drive

A machine model of a PM synchronous motor can be described in a rotor rotating [11] as follows:

$$v_q = R_s i_q + p\lambda_q + w_s\lambda_d, \tag{10}$$

$$v_d = R_s i_d + p\lambda_d - w_s\lambda_q, \tag{11}$$

where

$$\lambda_q = L_q i_q, \tag{12}$$

$$\lambda_d = L_d i_d + L_{md} I_{fd}. \tag{13}$$

In the above equations, v_d and v_q are the d and q axis stator voltages, i_d and i_q are the d and q axis stator currents, L_d and L_q are the d and q axis inductances, λ_d and λ_q are the d and q axis stator flux linkages and R_s and w_s are the stator resistance and inverter frequency, respectively. In Eq. (13), I_{fd} is the equivalent d-axis magnetizing current and L_{md} is the d-axis mutual inductance. The electric torque is

$$\tau_m = \tfrac{3}{2}p[L_{md} I_{fd} i_q + (L_d - L_q) i_d i_q] \tag{14}$$

and the equation for the motor dynamics is

$$\tau_e = \tau_m + B_m\omega_r + J_m\dot{\omega}_r. \tag{15}$$

In Eq. (14), p is the number of pole pairs, τ_m is the load torque, B_m is the damping coefficient, ω_r is the rotor speed and J_m is the moment of inertia. The basic principle in controlling a PM synchronous motor drive is based on field orientation. The flux position in the d–q coordinates can be determined by the shaft-position sensor because the magnetic flux generated from the rotor permanent magnetic is fixed in relation to the rotor shaft position. In Eqs. (13–14), if $i_d = 0$, the d-axis flux linkage λ_d is fixed since L_{md} and I_{fd} are constant for a surface-mounted PM synchronous motor, and the electromagnetic torque τ_e is then proportional to i_q, which is determined by closed-loop control. The rotor flux is produced in the d-axis only, and the current vector is generated in the q-axis for the field-oriented control. As the generated motor torque is linearly proportional to the q-axis current as the d-axis rotor flux is constant in Eq. (14), the maximum torque per ampere can be achieved. With the implementation of field-oriented control, the PM synchronous motor drive system can be simplified to a control system block diagram, as shown in Fig. 2, in which

$$\tau_e = K_t i_q^*, \tag{16}$$

$$K_t = \tfrac{3}{2} P L_{md} I_{fd}, \tag{17}$$

$$H_p(s) = \frac{1}{J_m s + B_m}, \tag{18}$$

where i_q^* is the torque current command. By substituting Eq. (16) into Eq. (15), the following applied torque can be obtained:

$$\tau_m = K_t i_q - J_m \dot{\omega}_r - B_m \omega_r, \tag{19}$$

where τ_m is the torque applied in the direction of ω_r, and the variables ω_r and $\dot{\omega}_r$ are the angular speed and acceleration of the disk, respectively.

2.2. Governing equations

Hamilton's principle, Lagrange multiplier, geometric constraints and partitioning method are employed to formulate the differential-algebraic equation (DAE) for a slider-crank mechanism. The angles θ and ϕ are selected as the generalized coordinates. The complete derivation of the equations of motion is given in Appendix A. By taking account of the control force and constraint

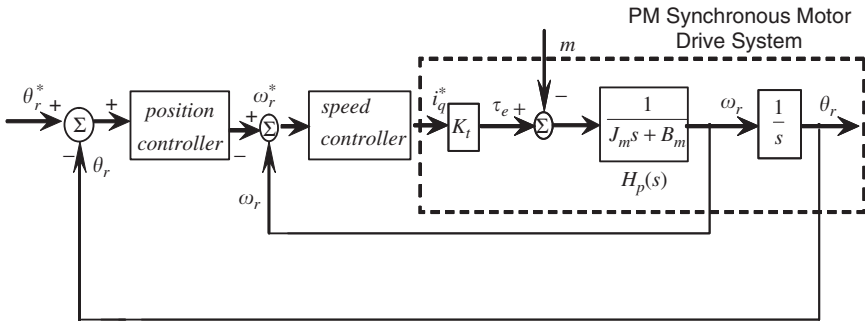

Fig. 2. The simplified control block diagram.

force, the equation in the matrix form can be obtained as

$$\mathbf{M}(\mathbf{Q})\ddot{\mathbf{Q}} + \mathbf{N}(\mathbf{Q}, \dot{\mathbf{Q}}) + \mathbf{\Phi}_{\mathbf{Q}}^{\mathrm{T}}\boldsymbol{\lambda} = \mathbf{Q}^{A}, \tag{20}$$

where $\mathbf{M}(\mathbf{Q})$, $\mathbf{N}(\mathbf{Q}, \dot{\mathbf{Q}})$, $\mathbf{\Phi}_{\mathbf{Q}}^{\mathrm{T}}\boldsymbol{\lambda}$ and $\mathbf{Q}^{A}$ can be seen in Appendix A.

2.3. Decouple the differential equations

In the dynamic analysis, the partitioning method [3,4] is employed, and the partitioning coordinate vector is selected as

$$\mathbf{Q} = [\mathbf{Q}_1 \ \mathbf{Q}_2 \ \cdots \ \mathbf{Q}_3]^{\mathrm{T}} = [\mathbf{p}^{\mathrm{T}} \ \mathbf{q}^{\mathrm{T}}]^{\mathrm{T}}, \tag{21}$$

where $\mathbf{p} = [p_1 \ p_2 \ \cdots \ p_m]^{\mathrm{T}}$ and $\mathbf{q} = [q_1 \ q_2 \ \cdots \ q_k]^{\mathrm{T}}$ are the m dependent and k independent coordinates, respectively. The m constraint equations are

$$\mathbf{\Phi}(\mathbf{Q}) \equiv \mathbf{\Phi}(\mathbf{p}, \mathbf{q}) = \mathbf{0}. \tag{22}$$

The numerical method may be used to solve the set of nonlinear algebraic equations (22). If the m constraint equations are independent, the existence of a solution $\mathbf{p}$ for a given $\mathbf{q}$ can be asserted by an implicit function theory.

Differentiating Eq. (22) yields the constraint velocity equation as

$$\mathbf{\Phi}_{\mathbf{Q}}\dot{\mathbf{Q}} = \mathbf{0}, \tag{23}$$

where matrix $\mathbf{\Phi}_{\mathbf{Q}} = [\partial\mathbf{\Phi}/\partial\mathbf{Q}]$ is the partial derivative of the constraint equation with respect to the coordinate, and is called the Jacobian constraint matrix. Sequentially, Eq. (23) can be rewritten in a partitioned form as

$$\mathbf{\Phi}_{\mathbf{p}}\dot{\mathbf{p}} = -\mathbf{\Phi}_{\mathbf{q}}\dot{\mathbf{q}}, \tag{24}$$

where $\mathbf{\Phi}_{\mathbf{p}}$ and $\mathbf{\Phi}_{\mathbf{q}}$ are two sub-matrices of $\mathbf{\Phi}_{\mathbf{Q}}$. Since the m constraint equations are assumed independent, $\mathbf{\Phi}_{\mathbf{p}}$ is an $m \times m$ nonsingular matrix. Sequentially, Eq. (21) can be solved directly for $\dot{\mathbf{p}}$ as long as $\dot{\mathbf{q}}$ is given.

Differentiating the constraint velocity of Eq. (23), the acceleration constraint equation becomes

$$\mathbf{\Phi}_{\mathbf{Q}}\ddot{\mathbf{Q}} = -(\mathbf{\Phi}_{\mathbf{Q}}\dot{\mathbf{Q}})_{\mathbf{Q}}\dot{\mathbf{Q}} \equiv \boldsymbol{\gamma}, \tag{25}$$

where $\ddot{\mathbf{Q}} = [\ddot{\mathbf{p}}^{\mathrm{T}} \ \ddot{\mathbf{q}}^{\mathrm{T}}]^{\mathrm{T}}$ is the vector of acceleration. Similarly, Eq. (25) can also be rewritten in a partitioned form as

$$\mathbf{\Phi}_{\mathbf{p}}\ddot{\mathbf{p}} = -\mathbf{\Phi}_{\mathbf{q}}\ddot{\mathbf{q}} - (\mathbf{\Phi}_{\mathbf{Q}}\dot{\mathbf{Q}})_{\mathbf{Q}}\dot{\mathbf{Q}}. \tag{26}$$

Since $\mathbf{\Phi}_{\mathbf{p}}$ is nonsingular, Eq. (26) can be solved for $\ddot{\mathbf{p}}$, once $\ddot{\mathbf{q}}$ is given. Note that the velocity (24) and acceleration (26) are two sets of linear algebraic equations in $\dot{\mathbf{Q}}$ and $\ddot{\mathbf{Q}}$, respectively.

Eqs. (20) and (25) can be combined into the matrix form as

$$\begin{bmatrix} \mathbf{M} & \mathbf{\Phi}_{\mathbf{Q}}^{\mathrm{T}} \\ \mathbf{\Phi}_{\mathbf{Q}} & \mathbf{0} \end{bmatrix} \begin{bmatrix} \ddot{\mathbf{Q}} \\ \boldsymbol{\lambda} \end{bmatrix} = \begin{bmatrix} \mathbf{Q}^{A} - \mathbf{N}(\mathbf{Q}, \dot{\mathbf{Q}}) \\ \boldsymbol{\gamma} \end{bmatrix}. \tag{27}$$

Eq. (27) represents a system of DAE and can be solved using the implicit function method as shown in the following reordering and partitioning processes.

Decomposing $\mathbf{Q}$ into $\mathbf{p}$ and $\mathbf{q}$, the system equations become

$$\mathbf{M}^{\mathbf{pp}}\ddot{\mathbf{p}} + \mathbf{M}^{\mathbf{pq}}\ddot{\mathbf{q}} + \boldsymbol{\Phi}_{\mathbf{p}}^{\mathrm{T}}\boldsymbol{\lambda} = \mathbf{Q}^{\mathbf{p}} - \mathbf{N}^{\mathbf{p}}, \tag{28a}$$

$$\mathbf{M}^{\mathbf{qp}}\ddot{\mathbf{p}} + \mathbf{M}^{\mathbf{qq}}\ddot{\mathbf{q}} + \boldsymbol{\Phi}_{\mathbf{q}}^{\mathrm{T}}\boldsymbol{\lambda} = \mathbf{Q}^{\mathbf{q}} - \mathbf{N}^{\mathbf{q}}, \tag{28b}$$

$$\boldsymbol{\Phi}_{\mathbf{p}}\ddot{\mathbf{p}} + \boldsymbol{\Phi}_{\mathbf{q}}\ddot{\mathbf{q}} = \boldsymbol{\gamma}. \tag{28c}$$

By using Eqs. (28a) and (28c) and eliminating $\boldsymbol{\lambda}$ and $\ddot{\mathbf{p}}$ we obtain

$$\boldsymbol{\lambda} = (\boldsymbol{\Phi}_{\mathbf{p}}^{\mathrm{T}})^{-1}[\mathbf{Q}^{\mathbf{p}} - \mathbf{N}^{\mathbf{p}} - \mathbf{M}^{\mathbf{pp}}\ddot{\mathbf{p}} - \mathbf{M}^{\mathbf{pq}}\ddot{\mathbf{q}}], \tag{29}$$

$$\ddot{\mathbf{p}} = \boldsymbol{\Phi}_{\mathbf{p}}^{-1}[\boldsymbol{\gamma} - \boldsymbol{\Phi}_{\mathbf{q}}\ddot{\mathbf{q}}]. \tag{30}$$

Eqs. (28b), (29) and (30) can be combined in the matrix form as

$$\hat{\mathbf{M}}(\mathbf{q})\ddot{\mathbf{q}} + \hat{\mathbf{N}}(\mathbf{q}, \dot{\mathbf{q}}) = \hat{\mathbf{F}}, \tag{31}$$

where

$$\hat{\mathbf{M}} = \mathbf{M}^{\mathbf{qq}} - \mathbf{M}^{\mathbf{qp}}\boldsymbol{\Phi}_{\mathbf{p}}^{-1}\boldsymbol{\Phi}_{\mathbf{q}} - \boldsymbol{\Phi}_{\mathbf{q}}^{\mathrm{T}}(\boldsymbol{\Phi}_{\mathbf{p}}^{\mathrm{T}})^{-1}[\mathbf{M}^{\mathbf{pq}} - \mathbf{M}^{\mathbf{pp}}\boldsymbol{\Phi}_{\mathbf{p}}^{-1}\boldsymbol{\Phi}_{\mathbf{q}}], \tag{32}$$

$$\hat{\mathbf{N}} = [\mathbf{N}^{\mathbf{q}} - \boldsymbol{\Phi}_{\mathbf{q}}^{\mathrm{T}}(\boldsymbol{\Phi}_{\mathbf{p}}^{\mathrm{T}})^{-1}\mathbf{N}^{\mathbf{p}}] + [\mathbf{M}^{\mathbf{qp}}\boldsymbol{\Phi}_{\mathbf{p}}^{-1} - \boldsymbol{\Phi}_{\mathbf{q}}^{\mathrm{T}}(\boldsymbol{\Phi}_{\mathbf{p}}^{\mathrm{T}})^{-1}\mathbf{M}^{\mathbf{pp}}\boldsymbol{\Phi}_{\mathbf{p}}^{-1}]\boldsymbol{\gamma}, \tag{33}$$

$$\hat{\mathbf{F}} = \mathbf{Q}^{\mathbf{q}} - \boldsymbol{\Phi}_{\mathbf{q}}^{\mathrm{T}}(\boldsymbol{\Phi}_{\mathbf{p}}^{\mathrm{T}})^{-1}\mathbf{Q}^{\mathbf{p}}. \tag{34}$$

For a slider-crank mechanism shown in Fig. 1(a), we have

$$\mathbf{p} = [\phi], \quad \mathbf{q} = [\theta],$$

$$\boldsymbol{\Phi}_{\mathbf{q}} = [r\cos\theta], \quad \boldsymbol{\Phi}_{\mathbf{p}} = [-l\cos\phi],$$

$$\mathbf{M}^{\mathbf{pp}} = [A], \quad \mathbf{M}^{\mathbf{pq}} = [E], \quad \mathbf{M}^{\mathbf{qp}} = [E], \quad \mathbf{M}^{\mathbf{qq}} = [B],$$

$$\mathbf{N}^{\mathbf{p}} = [K_W], \quad \mathbf{N}^{\mathbf{q}} = [P_W],$$

$$\mathbf{Q}^{\mathbf{p}} = [(F_B + F_E)l\sin\phi], \quad \mathbf{Q}^{\mathbf{q}} = [(F_B + F_E)r\sin\theta - \tau],$$

where A, B, E, K_W and P_W can be seen in Appendix A.

Eq. (31) is a set of differential equations with only one independent generalized coordinate vector $\mathbf{q} = [\theta]$. It is seen that the entries of $\hat{\mathbf{M}}$, $\hat{\mathbf{N}}$ and $\hat{\mathbf{F}}$ of Eq. (31) have two independent variables θ and ϕ. By using Eq. (4) and its time derivative, we could derive the equation with only one independent variable θ as follows:

$$\hat{M}(\theta)\ddot{\theta} + \hat{N}(\theta, \dot{\theta}) = \hat{F}(\theta), \tag{35}$$

where

$$\hat{M} = \left[(2m_3 + m_2) + \frac{m_3}{c} r\cos\theta\right]\left(\frac{r^3}{c}\cos\theta\sin^2\theta\right) + (m_2 + m_3)r^2\sin^2\theta + \frac{1}{3}m_2\left(\frac{l}{c}\right)^2(r\cos\theta)^2 + \frac{1}{2}m_1r^2 + J_m,$$

$$\hat{N} = \left\{m_2r^2\sin\theta\cos\theta\left[1 - \frac{l^2}{3c^2} + \frac{r}{c}\cos\theta + \frac{(lr)^2}{3c^4}\cos^2\theta + \frac{r^3}{2c^3}\cos\theta\sin^2\theta\right] - m_2\frac{r^3}{2c}\sin^3\theta + m_3r^2\sin\theta\cos\theta\left[1 - \frac{r^2}{c^2}\sin^2\theta + \frac{r^2}{c^2}\cos^2\theta + \frac{2r}{c}\cos\theta + \frac{r^4\cos^2\theta\sin^2\theta}{c^4} + \frac{r^3}{c^3}\sin^2\theta\cos\theta\right] - m_3\frac{r^3}{c}\sin^3\theta\right\}\dot{\theta}^2 + B_m\dot{\theta} + \frac{1}{2}m_2gr\cos\theta,$$

$$\hat{F} = K_ti_q - (F_B + F_E)r\sin\theta\left(1 + \frac{r}{c}\cos\theta\right),$$

$$c = \sqrt{l^2 - r^2\sin^2\theta}.$$

The system becomes an initial value problem and can be directly integrated by using the fourth-order Runge–Kutta method.

2.4. Alternative dynamic modeling

An alternative dynamic modeling by the Euler–Lagrange equation is shown in Appendix B, and the dynamic equation obtained in terms of only one independent variable θ is the same as that of Eq. (35).

3. Identification based on real-coded genetic algorithm

The parameters of a slider-crank mechanism could not be obtained directly. In order to solve the arduous problem, the RGA is employed to find the optimal identified parameters of a slider-crank mechanism. Therefore, the unknown parameters m_1, m_2, m_3, r and l could be identified by the input current i_q and output θ, $\dot{\theta}$ and $\ddot{\theta}$.

3.1. The procedure of the real-coded genetic algorithm

The procedure of the RGA [9] is shown in Fig. 3 and is described as follows.

Step 1: *Setting the constraint specification*. Before executing the RGA process, some specifications must be decided for the RGA, i.e. population size, maximum generation number, crossover probability, mutation probability, the fitness function, the range of each parameter, etc. Note that the setting specifications must be reasonable, because good initial parameters and specifications dramatically speed up the convergence. In this study, we can assign the searching range of the elements by our knowledge and experience.

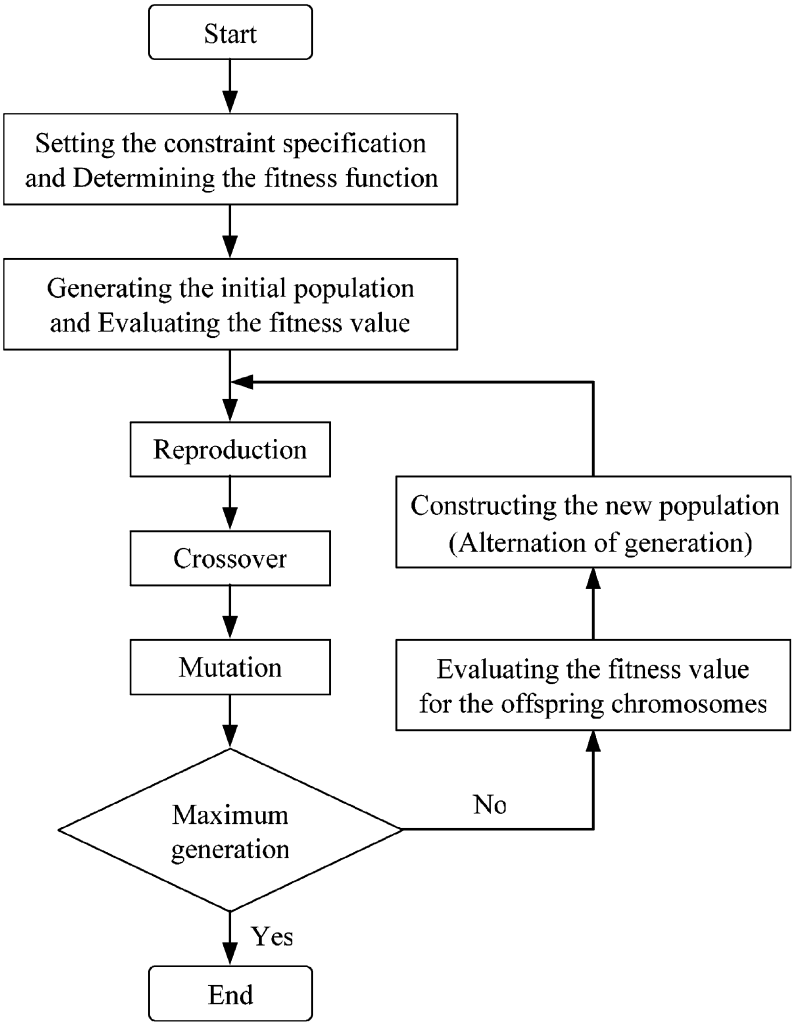

Fig. 3. The flow chart of the genetic algorithm.

Step 2: *Determining fitness function*. How to define the fitness function is the key point of the genetic algorithm, since the fitness function is a figure of merit, computed by using any domain knowledge. First, Eq. (35) can be rewritten as follows:

$$E = \hat{M}(\theta) \cdot \ddot{\theta} + \hat{N}(\theta, \dot{\theta}) - \hat{F}(\theta) = 0. \tag{36}$$

Then, the fitness function can defined as

$$F_f(m_1, m_2, m_3, r, l) = \frac{D}{\sum_{i=1}^{n} E_i^2}, \tag{37a}$$

$$E_i = |\hat{M}_i(\theta_i) \cdot \ddot{\theta}_i + \hat{N}_i(\theta_i, \dot{\theta}_i) - \hat{F}_i(\theta_i)|, \tag{37b}$$

where D is a positive constant, E_i are the calculated value and tested value of the ith sample point of E in time domain, n is the number of samples, and θ_i, $\dot{\theta}_i$ and $\ddot{\theta}_i$ are all tested values.

Step 3: *Generating the initial population*. According to the constraint, determine the range of each parameter; then the initial real-valued genes in chromosomes are generated by a sequence of real-valued variable by the range we limited randomly.

In this study, there are 5 parameters. The population size is 200. Then, the chromosomes P_1 and P_2 are expressed as

$$P_1 = (m_{11}, m_{21}, m_{31}, r_1, l_1), \tag{38a}$$

$$P_2 = (m_{12}, m_{22}, m_{32}, r_2, l_2), \tag{38b}$$

where m_{11} and m_{12}, m_{21} and m_{22}, m_{31} and m_{32}, r_1 and r_2, l_1 and l_2, are the genes of the variables m_1, m_2, m_3, r and l, respectively. The crossover (step 6) and mutation (step 7) are carried out between m_{11} and m_{12}, m_{21} and m_{22}, m_{31} and m_{32}, r_1 and r_2, l_1 and l_2.

Step 4: *Evaluating fitness value*. The fitness function has already been defined in step 2. The fitness value of each chromosome is obtained by calculating the fitness value according to step 2.

Step 5: *Reproduction*. The reproduction procedure adopts the roulette wheel selection to pick chromosomes into the mating pool. Therefore, the probability of the jth chromosome into the mating pool uses the following equation:

$$\text{fit\_ratio}_j = \frac{\text{fitness\_value}_j}{\sum_{j=1}^{200} \text{fitness\_value}}. \tag{39}$$

The chromosomes of the mating pool are called parent chromosomes, which are randomly selected by probability. In general, it is easier for the superior chromosomes to enter the mating pool. The reproduction module is a preparation before execution of the crossover procedure.

Step 6: *Crossover*. Crossover recombines the genetic material in two randomly selected parent chromosomes from the mating pool to produce two children (offspring). Here, the arithmetic crossover operator [9] is used, which is defined as follows:

$$x_{01} = (1 - \alpha) \cdot x_{p1} + \alpha \cdot x_{p2}, \tag{40a}$$

$$x_{02} = \alpha \cdot x_{p1} + (1 - \alpha) \cdot x_{p2}, \tag{40b}$$

where x_{p1} and x_{p2} are two genes in parent chromosomes, x_{01} and x_{02} are two children, and α is selected randomly between 0 and 1. The crossover probability is generally given between 0.8 and 1. In this study, the crossover probability is 1.

Step 7: *Mutation*. Mutation is directly applied to the offspring genes. Here, uniform mutation is used, which is defined as follows:

$$x_{\text{new}} = LB + \beta(UB - LB), \tag{41}$$

where x_{new} is the gene after mutation, β is selected randomly between 0 and 1, LB is the minimum value of the gene's range and UB is the maximum value of the gene's range. The mutation procedure is executed by the mutation probability. In general, the mutation probability is often given a low value. In this study, the mutation probability is 0.08.

Step 8: *Evaluating fitness value for offspring chromosomes*. Through the operators of steps 3–7, the new chromosomes can be obtained, which are called the "offspring chromosomes". Then,

Eq. (37a) is employed to calculate the fitness value for the offspring chromosomes. However, the fitness value of offspring chromosomes may be inferior to that of their parents.

Step 9: *Constructing the new population*. In this step, the objective is to generate a new population (new parent chromosomes), which is composed of superior chromosomes of parent and offspring population. The new population generating process is called ''generation'' or ''selection''.

Finally, the steps 5–9 are separated to search for the optimal solution until the end of the maximum generation. In this study, the maximum generation number is 100.

4. Identification based on the RLS

In this section, the RLS method is employed to identify the parameters of a slider-crank mechanism and the results will be compared with those by the RGA.

4.1. Least-squares algorithm

The standard form for a linear least-squares (LS) problem is given as

$$\mathbf{y} = \mathbf{X}\boldsymbol{\alpha} + \boldsymbol{\varepsilon} \quad \text{or } \mathbf{y} \cong \mathbf{X}\boldsymbol{\alpha}, \tag{42}$$

where $\mathbf{y}$ is a vector of noise-free measurements, $\boldsymbol{\varepsilon}$ is a vector of measurement noise, the matrix $\mathbf{X}$ contains known variables and parameters and $\boldsymbol{\alpha}$ is a vector of parameters to be identified. The symbol $\cong$ in $\mathbf{y} \cong \mathbf{X}\boldsymbol{\alpha}$ indicates that the left and right sides of Eq. (42) would be equal if noise was not present. The LS identification solution, $\hat{\boldsymbol{\alpha}}$, minimizes the sum of the squares of the error, $\mathbf{y} - \mathbf{X}\hat{\boldsymbol{\alpha}}$. If the problem at hand can be put into this standard form, by using a batch algorithm, $\hat{\boldsymbol{\alpha}}$ can be solved directly as

$$\hat{\boldsymbol{\alpha}} = (\mathbf{X}^{\mathrm{T}}\mathbf{X})^{-1}\mathbf{X}^{\mathrm{T}}\mathbf{y}, \tag{43}$$

if and only if $\mathbf{X}^{\mathrm{T}}\mathbf{X}$ is nonsingular, and Eq. (43) can be rewritten as

$$\hat{\alpha}(t) = \left(\sum_{i=1}^{t} x(i)x^{\mathrm{T}}(i)\right)^{-1}\left(\sum_{i=1}^{t} x(i)y(i)\right) = p(t)\left(\sum_{i=1}^{t} x(i)y(i)\right). \tag{44}$$

Manipulating the original equations into the form $\mathbf{y} \cong \mathbf{X}\boldsymbol{\alpha}$ such that the standard LS solution can be solved is often the primary challenge, and requires careful, application-dependent decisions regarding approximations.

4.2. Recursive LS algorithm

In the study of the LS problem, Bjork [12] demonstrated that if $\mathbf{X}^{\mathrm{T}}\mathbf{X}$ is nonsingular, Eq. (43) has the following recursive solutions:

$$\hat{\boldsymbol{\alpha}}(t+1) = \hat{\boldsymbol{\alpha}}(t) + \mathbf{K}(t+1)[\mathbf{y}(t+1) - \mathbf{x}^{\mathrm{T}}(t+1)\hat{\boldsymbol{\alpha}}(t)], \tag{45}$$

$$\mathbf{K}(t+1) = \mathbf{P}(t)\mathbf{x}(t+1)[\mathbf{I} + \mathbf{x}(t+1)\mathbf{P}(t)\mathbf{x}(t+1)]^{-1}, \tag{46}$$

$$\mathbf{P}(t+1) = \mathbf{P}(t) - \mathbf{P}(t)\mathbf{x}(t+1)[\mathbf{I} + \mathbf{x}(t+1)\mathbf{P}(t)\mathbf{x}^{\mathrm{T}}(t+1)]^{-1}\mathbf{x}^{\mathrm{T}}(t+1)\mathbf{P}(t), \tag{47}$$

where the last equality in Eq. (47) follows from the Matrix Inversion Lemma [13].

The recursive Eq. (47) plays a crucial role in the recursion Eqs. (45)–(47), and generally, when $\mathbf{X}^{\mathrm{T}}\mathbf{X}$ is singular, there exists no recursion similar to Eqs. (45)–(47). Comparing with the batch solution (43) the recursive solutions (45)–(47) offer important advantages. The RLS requires a constant computation time for each parameter update, and therefore it is perfectly suited for online use in real-time applications.

4.3. Derivation of the parameters for the RLS algorithm

The final dynamic equation of a slider-crank mechanism in matrix form is Eq. (35). In this paper, the goal of estimation parameters m_1, m_2, m_3, r and l is required to be written as vector. However, the parameters r and l cannot be expanded as a standard form of Eq. (42). Eq. (35) could only be modified as

$$y = [x_1 \;\; x_2 \;\; x_3] \begin{bmatrix} m_1 \\ m_2 \\ m_3 \end{bmatrix} = \mathbf{X}\hat{\boldsymbol{\alpha}}. \tag{48}$$

The details of the variables y, x_1, x_2 and x_3 are written in Appendix C. The $\hat{\boldsymbol{\alpha}}$ is the goal of identifying parameters by the RLS algorithm. By manipulating Eqs. (45–47), the input is the current i_q^* and the outputs are θ, $\dot{\theta}$ and $\ddot{\theta}$.

5. Numerical simulation and experimental results

5.1. Experimental setup

A block diagram of the computer control system for the PM synchronous servomotor drive coupled with a slider-crank mechanism is shown in Fig. 4(a) and the experimental equipment of a slider-crank mechanism of a computer control system is shown in Fig. 4(b). The control algorithm is implemented using a Pentium computer and the control software is LABVIEW. The PM synchronous servomotor is implemented by MITSUBISHI HC-KFS43 series. The specifications are shown as follows: rated output 400 (W), rated torque 1.3 (Nm), rated rotation speed 3000 (rev/min) and rated current 2.3 (A). The servo is implemented by MITSUBISHI MR-J2S-40A1. The control system is Sine-wave PWM control, which is a current control system. In order to measure the angle and angular speed of the disk and the position and velocity of the slider B, the interface of the device is implemented by motion control card PCI-7342. It can measure the angle of the disk and the position of slider B at the same time.

The main parameters of a slider-crank mechanism and servomotor used in the numerical simulations and the experiments are as follows:

$$m_1 = 0.232\,\mathrm{kg}, \quad m_2 = 0.332\,\mathrm{kg}, \quad m_3 = 0.600\,\mathrm{kg}, \quad r = 0.030\,\mathrm{m},$$

$$l = 0.217\,\mathrm{m}, \quad F_B = 0.100\,\mathrm{N}, \quad F_E = 0.000\,\mathrm{N}, \quad i_q = 0.400\,\mathrm{A},$$

$$K_t = 0.5652\,\mathrm{Nm/A}, \quad J_m = 6.700 \times 10^{-5}\,\mathrm{Nm\,s^2}, \quad B_m = 1.430 \times 10^{-2}\,\mathrm{Nm\,s/rad}.$$

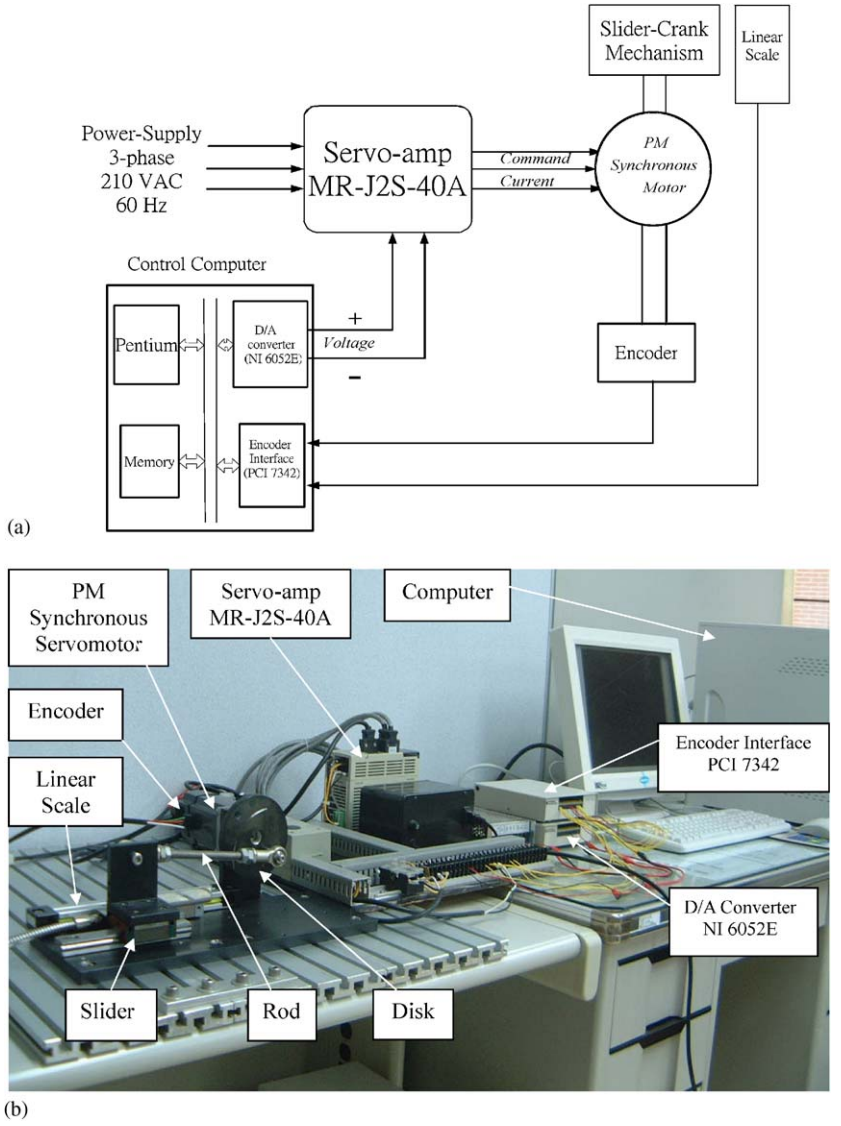

Fig. 4. The experimental setup. (a) Computer control system block diagram, (b) the experiment equipment of a slider-crank mechanism of the Computer control system.

5.2. Comparisons of the numerical and experimental results

Eq. (35) is calculated by the Runge–Kutta method with time step $\Delta t = 0.001$ s from 0 to 2 s to obtain the numerical solutions, which are compared with the experimental results of a slider-crank mechanism, and shown in Figs. 5(a), (b) and (c) for the angle θ, the angular speed $\dot{\theta}$ and the angular acceleration $\ddot{\theta}$ of the rigid disk, respectively. The angle θ and angular speed $\dot{\theta}$ are measured from the encoder directly, and the angular acceleration $\ddot{\theta}$ is numerically calculated from the angular speed $\dot{\theta}$. The displacement, speed and acceleration of a slider are shown in Figs. 5(d),

(e) and (f), respectively. The displacement x_B and speed $\dot{x}_B$ are measured from the linear scale directly, while the acceleration is numerically calculated from the speed. It is seen that the responses θ, $\dot{\theta}$, x_B and $\dot{x}_B$ between the numerical and experimental results nearly match. Therefore, the simulation responses of a slider-crank mechanism are well predicted by the experimental results.

5.3. The identification of a slider-crank mechanism

5.3.1. Numerical results

The θ_i, $\dot{\theta}_i$ and $\ddot{\theta}_i$ in Eq. (37b) are calculated by the Runge–Kutta method with time step $\Delta t = 0.001$ s from 0 to 2 s. The parameters m_1, m_2, m_3, r and l are identified by using the RGA method and the identified results are given in Table 1. From Fig. 6, it is seen that the fitness value

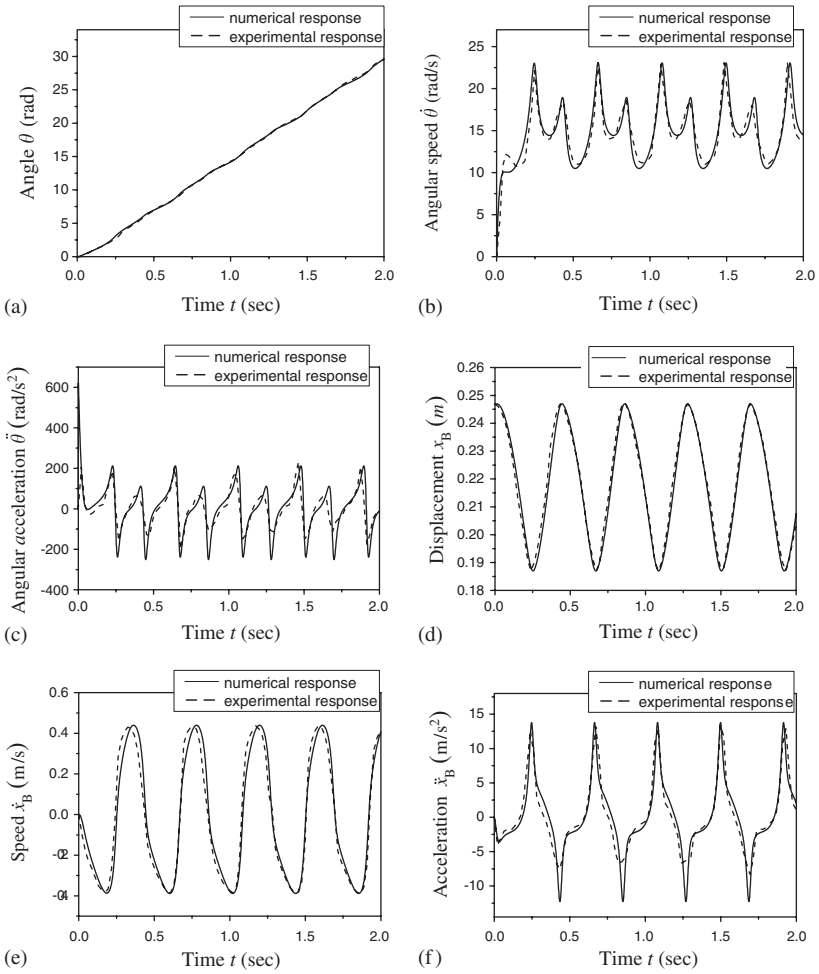

Fig. 5. Comparisons of the numerical and the experimental dynamic responses of a slider-crank mechanism.

increases with an increase in the value of the generation number, and the genes (m_1, m_2, m_3, r, l) of the chromosome almost converge well near the 40th generation. Fig. 7 shows the comparisons of the numerical dynamic responses and the identified dynamic responses of a slider-crank mechanism. They are almost the same.

5.3.2. Experimental results

The θ_i, $\dot{\theta}_i$, and $\ddot{\theta}_i$ in Eq. (37b) are obtained from experiments with time step $\Delta t = 0.02$ s from 0 to 2 s. Similarly, the parameters m_1, m_2, m_3, r and l are identified using the method based on RGA, and the identified results are given in Fig. 8 and Table 2. From Fig. 8, it is seen that the fitness value increases with an increase in the value of the generation number; however, the genes (m_1, m_2, m_3, r, l) of the chromosome almost converge well near the 60th generation.

In order to improve the defect, the damping effect is added to the dynamic equation (35). Following the similar process, Eq. (42) is obtained as follows:

$$\widehat{M}(\theta)\ddot{\theta} + \widehat{N}(\theta, \dot{\theta}) + C_d \cdot \dot{\theta} = \hat{F}(\theta). \tag{49}$$

The fitness function can be defined as follows:

$$F_f(m_1, m_2, m_3, r, l, C_d) = \frac{D}{\sum_{i=1}^{n} E_i^2}, \tag{50a}$$

where

$$E_i = |\hat{M}_i(\theta_i) \cdot \ddot{\theta}_i + \hat{N}_i(\theta_i, \dot{\theta}_i) + C_d \cdot \dot{\theta}_{\cdot i} - \hat{F}_i(\theta_i)|. \tag{50b}$$

The parameters m_1, m_2, m_3, r, l and C_d are identified again. The identified results are also given in Fig. 8 and Table 2 for comparison with those without damping effect. The genes $(m_1, m_2, m_3, r, l, C_d)$ of the chromosome also converge near the 60th generation. In these two cases, the constant values of D in Eqs. (37a) and (50a) are chosen such that the value of the fitness function is 1. It is seen that the identified parameters are very close for the system with and without damping.

Figs. 9(a) and (b) show the comparisons of the experimental results with the identified dynamic responses of a slider-crank mechanism with and without damping. It is found that the identified dynamic responses match the experimental results well if the damping effect is considered. Note

Table 1
The identified parameters of the numerical simulations

Parameter	m_1 (kg)	m_2 (kg)	m_3 (kg)
Feasible domain	0.000–1.000	0.000–1.000	0.000–1.000
The actual value	0.232	0.332	0.600
The identified value	0.234	0.331	0.603

Parameter	r (m)	l (m)
Feasible domain	0.000–0.100	0.000–1.000
The actual value	0.030	0.217
The identified value	0.030	0.216

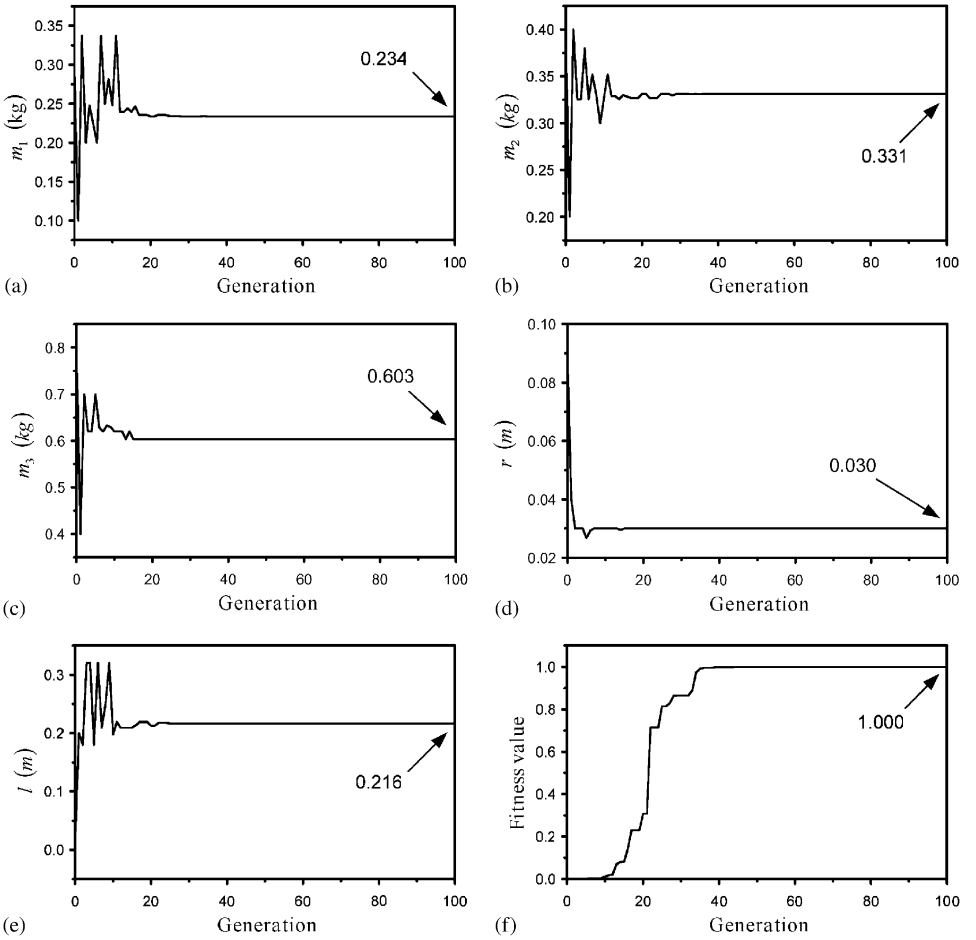

Fig. 6. The evolution history of the numerical identified parameters and fitness value.

that although the identified parameters may be different from the true system as seen in Table 2, the identified dynamic responses agree well with the experimental results. Therefore, the identified parameters can be called the equivalent parameters and they are feasible.

5.3.3. *Comparison between the RGA and RLS*

In this section, the identified dynamic responses by the RGA and RLS will be compared with the experimental results. The LS standard form of Eq. (42) for a slider-crank mechanism with damping can be modified as follows:

$$y = [x_1 \;\; x_2 \;\; x_3 \;\; x_4] \begin{bmatrix} m_1 \\ m_2 \\ m_3 \\ C_d \end{bmatrix} = \mathbf{X}\hat{\boldsymbol{\alpha}}, \tag{51}$$

where y, x_1, x_2, x_3 and x_4 are given in Appendix C.

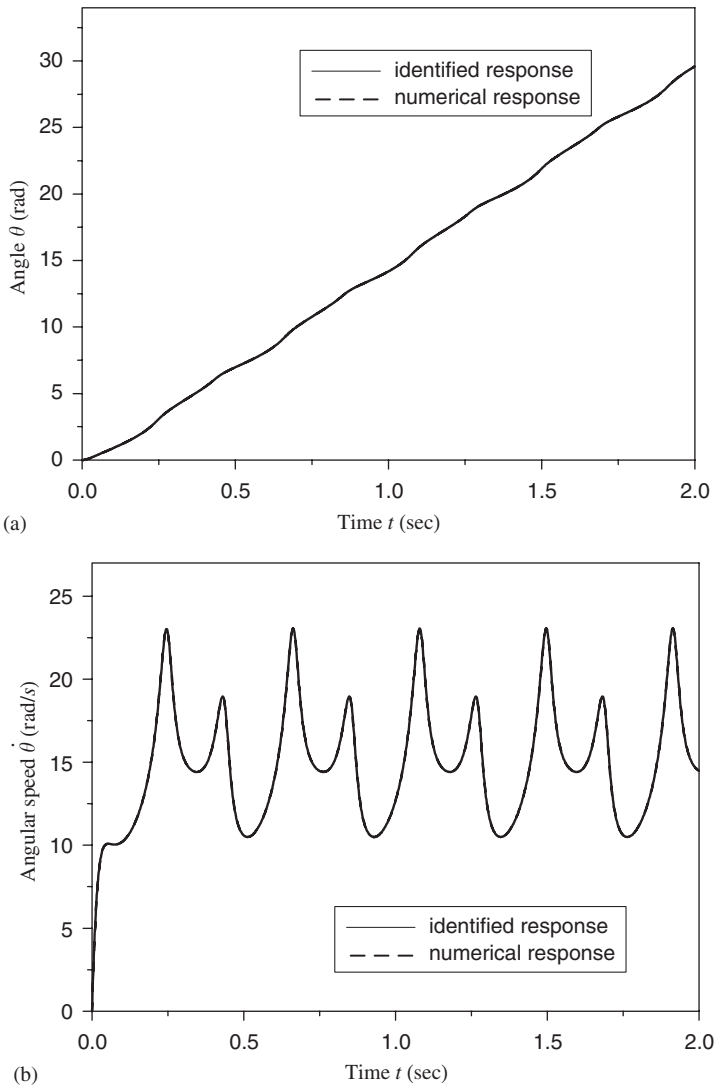

Fig. 7. Comparisons of the numerical and the identified dynamic responses of a slider-crank mechanism.

With an input current $i_q = 0.4\,\mathrm{A}$, the disk variations θ, $\dot{\theta}$ and $\ddot{\theta}$ are experimentally obtained with time step $\Delta t = 0.02\,\mathrm{s}$ from 0 to 4 s. It is noted that only the angle θ and angular speed $\dot{\theta}$ of the disk can be experimentally measured by the encoder; its angular acceleration $\ddot{\theta}$ is numerically calculated from the angular speed. Sequentially, the unknown parameters of a slider-crank mechanism are identified by substituting them into Eqs. (45)–(47) and using the RLS algorithm. Finally, the experimentally identified parameters are obtained as follows: $m_1 = 0.114\,\mathrm{kg}$, $m_2 = 0.11\,\mathrm{kg}$, $m_3 = 0.818\,\mathrm{kg}$ and $C_d = 1.17 \times 10^{-3}\,\mathrm{N\,s/rad}$. By using these experimentally identified parameters in the RGA and RLS, we obtain the dynamic responses of a slider-crank mechanism by numerical computations of Eq. (49). The angle and its angular

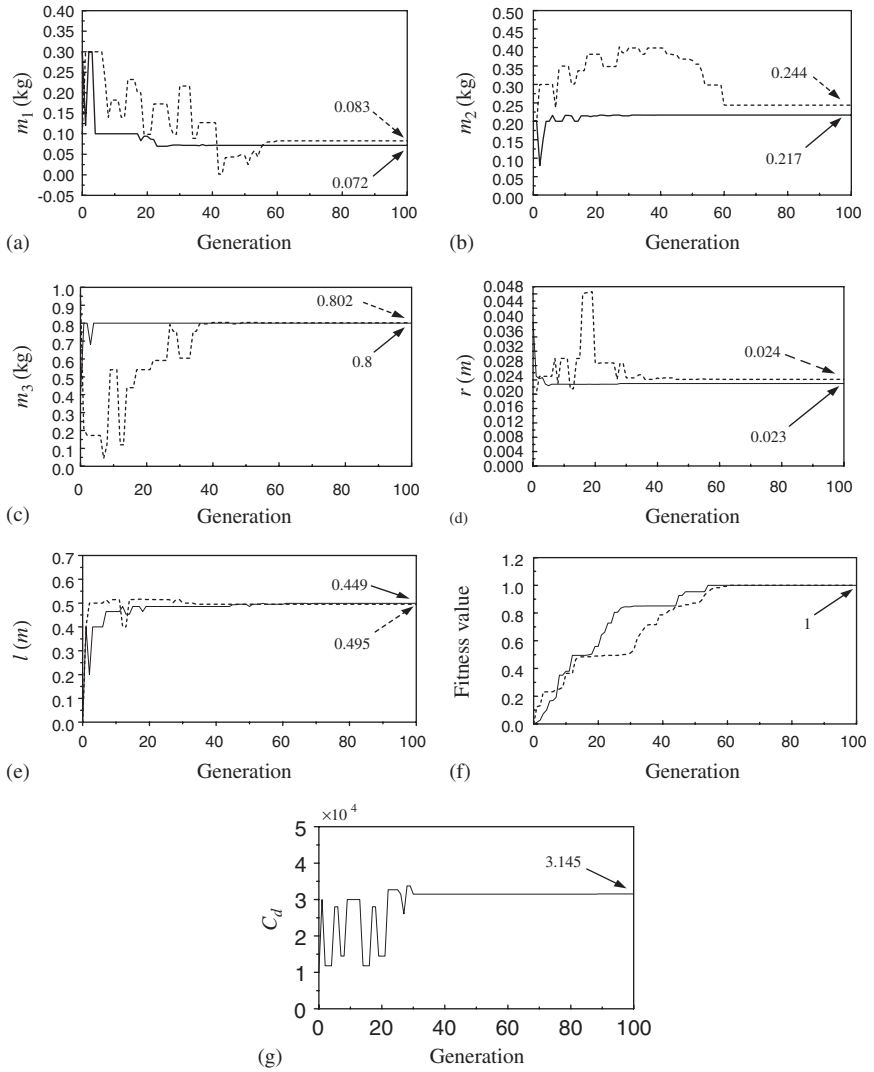

Fig. 8. The evolution history of the experimentally identified parameters and fitness value (without and with damping).

speed of the disk by the RGA and RLS are compared with the experimental results in Figs. 10(a) and (b), respectively. Observing the compared results, it is found that the responses by the RGA are closer to the experimental results than those by the RLS. However, the computational times performed by the same personal computer are about 3 s by the RLS online and 50 s by the RGA off-line for the identified parameters being converged stably.

In conclusion, it is seen that the dynamic responses θ and $\dot{\theta}$ by the RGA are in good agreement with experimental results. In other words, the dynamic responses of a slider-crank mechanism are predicted well and its parameters are identified accurately by the RGA.

Table 2
The identified parameters of the experimentations with (without) damping

Parameter	m_1 (kg)	m_2 (kg)	m_3 (kg)
Feasible domain	0.000–1.000	0.000–1.000	0.000–1.000
The identified value	0.083 (0.072)	0.224 (0.217)	0.802 (0.800)
Parameter	r (m)	l (m)	C_d
Feasible domain	0.000–0.100	0.000–1.000	0.000–0.001
The identified value	0.024 (0.023)	0.495 (0.499)	3.145×10^{-4}

6. Conclusions

The dynamic formulations of a slider-crank mechanism driven by a field-oriented PM synchronous motor drive have been successfully formulated with only one independent variable. The dynamic formulation can give a good interpretation of a slider-crank mechanism by comparing the numerical simulations with experimental results. Furthermore, a new identified method using the real-coded genetic algorithm is employed to search the parameters of a slider-crank mechanism. The responses are compared with those by the RLS and the experimental results. It is found that the responses by the RGA are closer to the experimental results than those by the RLS, but the time needed for off-line computation by the RGA is longer than that needed by the RLS online.

Acknowledgements

The financial support from the National Science Council of the Republic of China with contract number NSC-92-2815-E-327-003 is gratefully acknowledged.

Appendix A. Dynamic formulation

The holomonic constraint equation of a slider-crank mechanism from Eq. (4) is obtained as

$$\mathbf{\Phi}(\mathbf{Q}) = r\sin\theta - l\sin\phi = 0, \tag{A.1}$$

where $\mathbf{Q} = [\phi \;\; \theta]^{\mathrm{T}}$ is the vector of generalized coordinates.

The kinetic energies of the disk with mass m_1, the connected rod with mass m_2 and the slider with mass m_3 are, respectively,

$$T_1 = \tfrac{1}{2} I_1 \dot{\theta}^2 = \tfrac{1}{2}(\tfrac{1}{2} m_1 r^2)\dot{\theta}^2 = \tfrac{1}{4} m_1 r^2 \dot{\theta}^2, \tag{A.2}$$

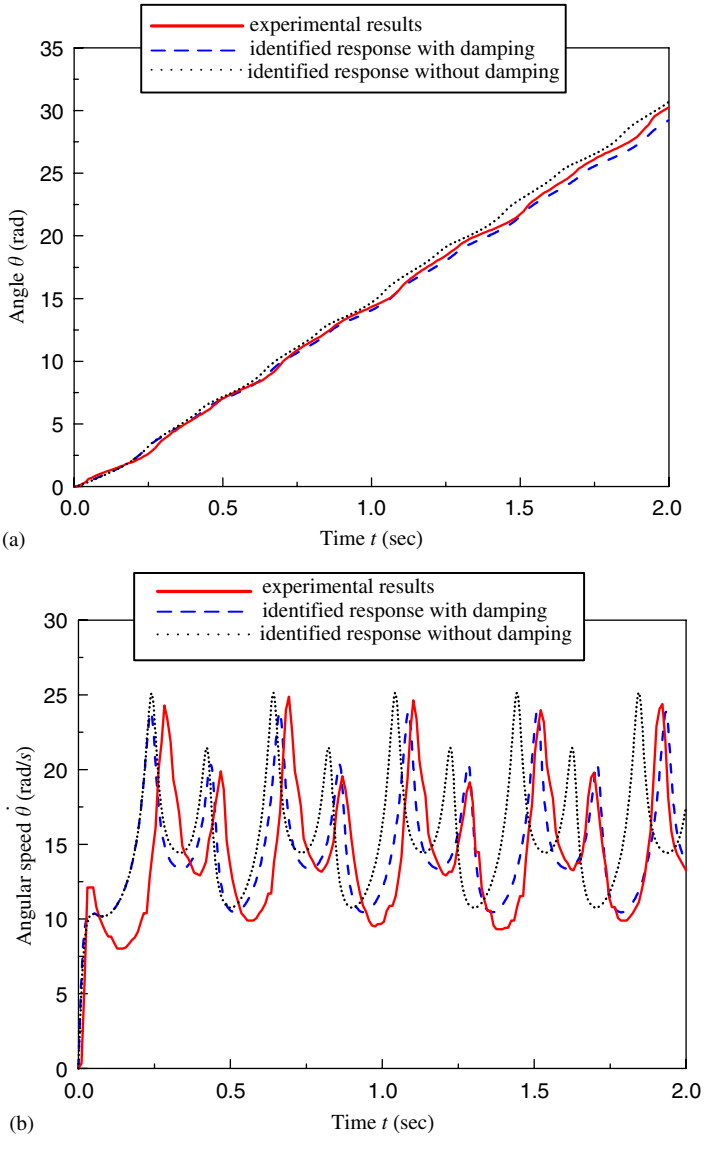

Fig. 9. Comparisons of the experimental results and the identified dynamic responses of a slider-crank mechanism.

$$T_2 = \tfrac{1}{2} I_2 \dot{\phi}^2 + \tfrac{1}{2} m_2 \dot{x}_{2cg}^2 + \tfrac{1}{2} m_2 \dot{y}_{2cg}^2$$
$$= \tfrac{1}{6} m_2 l^2 \dot{\phi}^2 + \tfrac{1}{2} m_2 r^2 \dot{\theta}^2 \sin^2\theta + \tfrac{1}{2} m_2 r l \dot{\theta}\dot{\phi} \sin\theta \sin\phi, \tag{A.3}$$

$$T_3 = \tfrac{1}{2} m_3 \dot{x}_3^2 = \tfrac{1}{2} m_3 r^2 \dot{\theta}^2 \sin^2\theta + m_3 r l \dot{\theta}\dot{\phi} \sin\theta \sin\phi + \tfrac{1}{2} m_3 l^2 \dot{\phi}^2 \sin^2\phi. \tag{A.4}$$

Then, the total kinetic energy of a slider-crank mechanism can be obtained as

$$T = T_1 + T_2 + T_3. \tag{A.5}$$

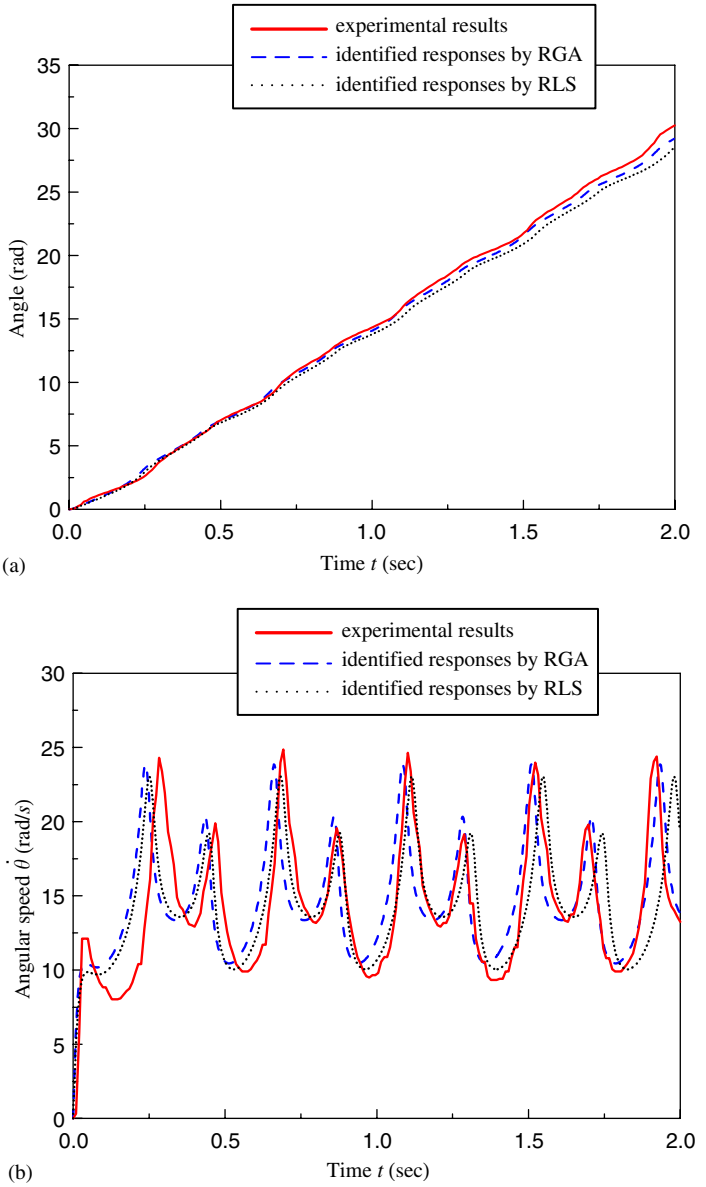

Fig. 10. Comparisons among the experimental results and the identified dynamic responses by the RGA and RLS for a slider-crank mechanism.

The gravitational potential energies V_1, V_2 and V_3 for the disk, connected rod and slider are, respectively,

$$V_1 = 0, \tag{A.6}$$

$$V_2 = m_2 g y_{2cg} = \tfrac{1}{2} m_2 g l \sin\phi, \tag{A.7}$$

$$V_3 = 0, \tag{A.8}$$

where g is the gravitational acceleration. The total potential energy of a slider-crank mechanism can be obtained as

$$V = V_1 + V_2 + V_3. \tag{A.9}$$

The virtual works δW^A done by the external disturbance force F_E and the friction force F_B with the virtual displacement δx of the slider, and the applied torque τ with the virtual angle $\delta\theta$ are summed as

$$\begin{aligned}\delta W^A &= \tau\delta\theta + (F_E + F_B)\delta x \\ &= \tau\delta\theta + (F_E + F_B)(-r\sin\theta\,\delta\theta - l\sin\phi\,\delta\phi) \\ &= -\delta\mathbf{Q}^{\mathrm{T}}\mathbf{Q}^A,\end{aligned} \tag{A.10}$$

where

$$F_B = -\mu m_B g\,\mathrm{sgn}(\dot{x}_B), \tag{A.11a}$$

$$\mathrm{sgn}(\dot{x}_B) = \begin{cases} 1 & \text{if } \dot{x}_B > 0, \\ 0 & \text{if } \dot{x}_B = 0, \\ -1 & \text{if } \dot{x}_B < 0, \end{cases} \tag{A.11b}$$

$$\mathbf{Q}^A = \begin{bmatrix} (F_E + F_B)l\sin\phi \\ (F_B + F_E)r\sin\theta - \tau \end{bmatrix} \tag{A.12}$$

and μ is the friction coefficient.

The virtual work δW^C done by the generalized constrained reaction force $\mathbf{Q}^C$ is

$$\delta W^c = \delta\mathbf{Q}^{\mathrm{T}}\mathbf{Q}^C, \tag{A.13}$$

where

$$\mathbf{Q}^C = \boldsymbol{\Phi}_{\mathbf{Q}}^{\mathrm{T}}\boldsymbol{\lambda},$$

$$\boldsymbol{\Phi}_{\mathbf{Q}} = \left[\frac{\partial\boldsymbol{\Phi}(\mathbf{Q})}{\partial\mathbf{Q}}\right] = [-l\cos\phi \;\; r\cos\theta]$$

and $\boldsymbol{\lambda}$ is the Lagrange multiplier.

The Lagrange function L can be written as

$$\begin{aligned}L &\equiv T - V \\ &= \tfrac{1}{4}m_1 r^2\dot{\theta}^2 + \tfrac{1}{6}m_2 l^2\dot{\theta}^2 + \tfrac{1}{2}m_2 r^2\dot{\theta}^2\sin^2\theta + \tfrac{1}{2}m_2 rl\dot{\theta}\dot{\phi}\sin\theta\sin\phi \\ &\quad + \tfrac{1}{2}m_3 r^2\dot{\theta}^2\sin^2\theta + m_3 rl\dot{\theta}\dot{\phi}\sin\theta\sin\phi + \tfrac{1}{2}m_3 l^2\dot{\phi}^2\sin^2\phi - \tfrac{1}{2}m_2 gl\sin\phi.\end{aligned} \tag{A.14}$$

Applying Hamilton's principle

$$0 = \int_{t_1}^{t_2}[\delta L + \delta W^A + \delta W^C]\,\mathrm{d}t = \int_{t_1}^{t_2}\delta\mathbf{Q}^{\mathrm{T}}\left[\frac{\partial L}{\partial\mathbf{Q}} - \frac{\mathrm{d}}{\mathrm{d}t}\frac{\partial L}{\partial\dot{\mathbf{Q}}} - \mathbf{Q}^A + \mathbf{Q}^C\right]\mathrm{d}t + \frac{\partial L}{\partial\dot{\mathbf{Q}}}\,\delta\mathbf{Q}\Big|_{t_1}^{t_2}. \tag{A.15}$$

We can obtain the Euler–Lagrange equation as follows:

$$\mathbf{M}(\mathbf{Q})\ddot{\mathbf{Q}} + \mathbf{N}(\mathbf{Q}, \dot{\mathbf{Q}}) + \mathbf{\Phi}_{\mathbf{Q}}^{\mathrm{T}}\boldsymbol{\lambda} = \mathbf{Q}^{A}, \tag{A.16}$$

where

$$\mathbf{M} = \begin{bmatrix} A & E \\ E & B \end{bmatrix}, \quad \mathbf{N} = \begin{bmatrix} K_W \\ P_W \end{bmatrix}$$

and

$$A = \tfrac{1}{3}m_2 l^2 + m_3 l^2 \sin^2\phi,$$

$$B = \tfrac{1}{2}m_1 r^2 + (m_2 + m_3) r^2 \sin^2\theta,$$

$$E = (\tfrac{1}{2}m_2 + m_3) rl \sin\theta \sin\phi,$$

$$K_W = m_3 l^2 \dot{\phi}^2 \sin\phi\cos\phi + (\tfrac{1}{2}m_2 + m_3) rl\dot{\theta}^2 \cos\theta \sin\phi + \tfrac{1}{2}m_2 gl \cos\phi,$$

$$P_W = (\tfrac{1}{2}m_2 + m_B) rl\dot{\phi}^2 \sin\theta\cos\phi + (m_2 + m_B) r^2\dot{\theta}^2 \sin\theta\cos\theta.$$

Appendix B. Alternative dynamic modeling of a slider-crank mechanism

In order to show that Eq. (35) is correct, the Euler–Lagrange equation will be applied in the following form:

$$\frac{\mathrm{d}}{\mathrm{d}t}\left(\frac{\partial L}{\partial \dot{\theta}}\right) - \frac{\partial L}{\partial \theta} = \mathbf{Q}^{A}. \tag{B.1}$$

First, applying the relation of θ and ϕ in Eq. (4), the kinetic energies T_1, T_2 and T_3 of Eqs. (A.2, A.3, A.4), respectively, rewritten in terms of θ and $\dot{\theta}$ are

$$T_1 = \tfrac{1}{2}I_1\dot{\theta}^2 = \tfrac{1}{4}m_1 r^2\dot{\theta}^2, \tag{B.2}$$

$$\begin{aligned} T_2 &= \tfrac{1}{2}I_2\dot{\phi}^2 + \tfrac{1}{2}m_2\dot{x}_{2cg}^2 + \tfrac{1}{2}m_2\dot{y}_{2cg}^2 \\ &= m_2\dot{\theta}^2\left[\frac{1}{6}\left(\frac{lr\cos\theta}{c}\right)^2 + \frac{1}{2}(r\sin\theta)^2 + \frac{1}{2}\frac{r^3}{c}\cos\theta\sin^2\theta\right], \end{aligned} \tag{B.3}$$

$$T_3 = \frac{1}{2}m_3\dot{x}_3^2 = m_3\dot{\theta}^2\left[\frac{1}{2}(r\sin\theta)^2 + \frac{r^3\sin^2\theta\cos\theta}{c} + \frac{1}{2}\frac{r^4\sin^2\theta\cos^2\theta}{c^2}\right], \tag{B.4}$$

$$c = \sqrt{l^2 - r^2\sin^2\theta}.$$

The gravitational potential energy V_2 of the connected rod is rewritten as

$$V_2 = m_2 g y_{2cg} = \frac{1}{2} m_2 g r \sin\theta. \tag{B.5}$$

The Lagrange function L is obtained as follows:

$$\begin{aligned} L &\equiv T - V \\ &= \frac{1}{4} m_1 r^2 \dot{\theta}^2 + m_2 \dot{\theta}^2 \left[\frac{1}{6} \frac{(lr)^2 \cos^2\theta}{c^2} + \frac{1}{2} (r\sin\theta)^2 + \frac{1}{2} \frac{r^3 \sin^2\theta \cos\theta}{c} \right] \\ &\quad + m_B \dot{\theta}^2 \left[\frac{1}{2} (r\sin\theta)^2 + \frac{r^3 \sin^2\theta\cos\theta}{c} + \frac{1}{2} \frac{r^4 \sin^2\theta\cos^2\theta}{c^2} \right] - \frac{1}{2} m_2 g r \sin\theta. \end{aligned} \tag{B.6}$$

The virtual works δW^A of Eq. (A.10) are rewritten as

$$\delta W^A = \tau\delta\theta + (F_E + F_B)\delta x = \left[\tau - (F_B + F_E)\left(1 + \frac{1}{c} r\cos\theta \right) r\sin\theta \right] \delta\theta. \tag{B.7}$$

Substituting Eqs. (B.6) and (B.7) into the Euler–Lagrange Eq. (B.1), we have

$$\begin{aligned} &\left\{ \left[(2m_3 + m_2) + \frac{m_3}{c} r\cos\theta \right] \left(\frac{r^3}{c} \cos\theta \sin^2\theta \right) + (m_2 + m_3) r^2 \sin^2\theta \right. \\ &\quad \left. + \frac{1}{3} m_2 \left(\frac{l}{c} \right)^2 (r\cos\theta)^2 + \frac{1}{2} m_1 r^2 + J_m \right\} \ddot{\theta} + \left\{ m_2 r^2 \sin\theta\cos\theta \left[1 - \frac{l^2}{3c^2} + \frac{r}{c}\cos\theta \right. \right. \\ &\quad \left. + \frac{(lr)^2}{3c^4} \cos^2\theta + \frac{r^3}{2c^3} \cos\theta \sin^2\theta \right] - m_2 \frac{r^3}{2c} \sin^3\theta + m_3 r^2 \sin\theta\cos\theta \left[1 - \frac{r^2}{c^2} \sin^2\theta \right. \\ &\quad \left. \left. + \frac{r^2}{c^2} \cos^2\theta + \frac{2r}{c} \cos\theta + \frac{r^4 \cos^2\theta \sin^2\theta}{c^4} + \frac{r^3}{c^3} \sin^2\theta\cos\theta \right] - m_3 \frac{r^3}{c} \sin^3\theta \right\} \dot{\theta}^2 \\ &\quad + B_m \dot{\theta} + \frac{1}{2} m_2 g r \cos\theta = K_t i_q - (F_B + F_E) r \sin\theta \left(1 + \frac{r}{c} \cos\theta \right), \end{aligned} \tag{B.8}$$

which is the same as Eq. (35), and has only one independent variable θ.

Appendix C. The RLS standard form of a slider-crank mechanism

Eq. (49) for a slider-crank mechanism with damping can be expressed in the LS standard form as follows:

$$y = [x_1 \;\; x_2 \;\; x_3 \;\; x_4] \begin{bmatrix} m_1 \\ m_2 \\ m_3 \\ C_d \end{bmatrix}, \tag{C.1}$$

where

$$y = K_t i_q - (F_B + F_E) r \sin\theta \left(1 + \frac{r\cos\theta}{\sqrt{l^2 - r^2\sin^2\theta}}\right) - B_m\dot{\theta} - J_m\ddot{\theta}, \tag{C.2}$$

$$x_1 = \frac{1}{2} r^2 \ddot{\theta}, \tag{C.3}$$

$$\begin{aligned} x_2 = {} & \frac{1}{2} gr\cos\theta + \dot{\theta}^2 r^2 \cos\theta\sin\theta + \ddot{\theta} r^2 \sin^2\theta + \frac{\dot{\theta}^2 l^2 r^4 \cos^3\theta\sin\theta}{3(l^2 - r^2\sin^2\theta)} \\ & + \frac{\dot{\theta}^2 r^5 \cos^2\theta\sin^3\theta}{2(l^2 - r^2\sin^2\theta)^{3/2}} + \frac{\ddot{\theta} l^2 r^2 \cos^2\theta}{3(l^2 - r^2\sin^2\theta)} - \frac{\dot{\theta}^2 l^2 r^2 \cos\theta\sin\theta}{3(l^2 - r^2\sin^2\theta)} \\ & + \frac{\dot{\theta}^2 r^3 \cos^2\theta\sin\theta}{\sqrt{(l^2 - r^2\sin^2\theta)}} + \frac{\ddot{\theta} r^3 \cos\theta\sin^2\theta}{\sqrt{(l^2 - r^2\sin^2\theta)}} - \frac{\dot{\theta}^2 r^3 \sin^3\theta}{2\sqrt{(l^2 - r^2\sin^2\theta)}}, \end{aligned} \tag{C.4}$$

$$\begin{aligned} x_3 = {} & \dot{\theta}^2 r^2 \cos\theta\sin\theta + \ddot{\theta} r^2 \sin^2\theta + \frac{\dot{\theta}^2 r^6 \cos^3\theta\sin^3\theta}{(l^2 - r^2\sin^2\theta)^2} \\ & + \frac{\dot{\theta}^2 r^5 \cos^2\theta\sin^3\theta}{(l^2 - r^2\sin^2\theta)^{3/2}} + \frac{\dot{\theta}^2 r^4 \cos^3\theta\sin\theta}{l^2 - r^2\sin^2\theta} + \frac{\ddot{\theta} r^4 \cos^2\theta\sin^2\theta}{l^2 - r^2\sin^2\theta} \\ & - \frac{\dot{\theta}^2 r^4 \cos\theta\sin^3\theta}{l^2 - r^2\sin^2\theta} + \frac{2\dot{\theta}^2 r^3 \cos^2\theta\sin\theta}{\sqrt{(l^2 - r^2\sin^2\theta)}} + \frac{2\ddot{\theta} r^3 \cos\theta\sin^2\theta}{\sqrt{(l^2 - r^2\sin^2\theta)}} \\ & - \frac{\dot{\theta}^2 r^3 \sin^3\theta}{\sqrt{(l^2 - r^2\sin^2\theta)}}, \end{aligned} \tag{C.5}$$

$$x_4 = \dot{\theta}. \tag{C.6}$$

References

[1] B.V. Viscomi, R.S. Arye, Nonlinear dynamic response of elastic slider-crank mechanism, *ASME Journal of Engineering for Industry* 93 (1971) 251–262.

[2] R.F. Fung, Dynamic response of the flexible connecting rod of a slider-crank mechanism with time-dependent boundary effect, *Computer & Structure* 63 (1) (1997) 79–90.

[3] R.F. Fung, F.J. Lin, J.S. Huang, Y.C. Wang, Application of sliding mode control with a low-pass filter to the constantly rotating slider-crank mechanism, *The Japan Society of Mechanical Engineers C* 40 (4) (1997) 717–722.

[4] F.J. Lin, R.F. Fung, Y.S. Lin, Adaptive control of slider-crank mechanism motion: simulation and experiments, *International Journal of System Science* 28 (12) (1997) 1227–1238.

[5] J.H. Holland, *Adaptation in Natural and Artificial Systems*, The University of Michigan Press, Ann Arbor, MI, 1975.

[6] D.E. Goldberg, *Genetic Algorithms in Search, Optimization and Machine Learning*, Addison-Wesley, Reading, MA, 1989.

[7] K.F. Man, K.S. Tang, S. Kwong, Genetic algorithms: concepts and applications, *IEEE Transactions on Industrial Electronics* 43 (5) (1996) 519–534.
[8] R.L. Haupt, S.E. Haupt, *Practical Genetic Algorithms*, Wiley Interscience, New York, 1998.
[9] A.A. Adewuya, New Methods in Genetic Search with Real-valued Chromosomes, Master's Thesis, Massachusetts Institute of Technology, Cambridge, 1996.
[10] J.W. Kim, S.W. Kim, P.G. Park, T.J. Park, On the similarities between binary-coded GA and real-coded GA in wide search space, in: *IEEE Evolutionary Computation*, *CEC '02. Proceedings of the 2002 Congress*, 2002, pp. 681–686.
[11] P.C. Krause, *Analysis of Electric Machinery*, McGraw-Hill, New York, 1986.
[12] A. Bjork, *Numerical Methods for Least Squares Problem*, SIAM, Philadelphia, 1996.
[13] M.S. Phatak, Recursive method for optimum GPS satellite selection, *IEEE Transactions on Aerospace and Electronic Systems* 37 (2001) 751–754.